Characterization and Estimation of Elevation-Azimuth Dispersion of Individual Path Components

Xuefeng Yin[1], Lingfeng Liu[1], Daniel K. Nielsen[1], Nicolai Czink[3,2] and Bernard H. Fleury[1,2]

[1]Department of Electronics Systems, Aalborg University, Aalborg, Denmark
[2]Forschungszentrum Telekommunikation Wien (ftw.), Vienna, Austria
[3]Institute of Communications and RF Engineering, Vienna University of Technology, Vienna, Austria

***Abstract*— In this contribution, the density function of the Fisher-Bingham-5 distribution is used to describe the shape of the elevation-azimuth power spectrum of individual path components in the radio channel response. The maximum likelihood estimator of the parameters of the power spectrum is derived and applied to measurement data. Preliminary results are presented which illustrate the applicability of the characterization method in real environments.**

***Index Terms*— Path component, power spectrum, Fisher-Bingham-5 distribution, maximum likelihood estimation.**

I. Introduction

Due to the heterogeneity of the propagation environment, the response of the radio channel is the superposition of a certain number of components. Each component, which we call a "path component", is contributed by an electromagnetic wave propagating along a path from the transmitter (Tx) to the receiver (Rx). Along this path, the wave interacts with a certain number of objects called scatterers. Due to the geometrical extent and the nonhomogeneous electromagnetic properties of the scatterers, a path may be dispersive in delay, direction of departure, direction of arrival, polarizations, as well as in Doppler frequency when the environment is time-variant. Thus, an individual path component may be spread in these dispersion dimensions.

In recent years, different methods have been proposed for estimation of dispersive characteristics of individual path components. Some of these methods make use of the assumption that the shape of the power spectrum of individual path components can be described using a density function of a probability distribution. In the case where dispersion in one dimension, e.g. azimuth of arrival (AoA), is considered, the shape of the AoA power spectrum can be described using the density function of the (truncated) Gaussian distribution [2], the uniform distribution confined within a certain azimuth range [1], and the von-Mises distribution [3].

Dispersion of individual path components in multiple dimensions are also investigated recently. In [4], dispersion of path components in AoA and delay is studied. The shape of the AoA-delay power spectrum is described using the product of the von-Mises density function and the exponential density function. These two functions are used to describe the shapes of the (conditional) power spectrum in AoA and in delay respectively. This method assumes that there is no dependence between AoA dispersion and delay dispersion for individual path components. In [5], the density function of a bivariate von-Mises-Fisher distribution is proposed to characterize the shape of the power spectrum of individual path components in azimuth of departure (AoD) and AoA. Furthermore, in [6] a 3-variate density function is derived and is used to describe the shape of the AoD-AoA-delay power spectrum. The latter two distributions have the common feature that they maximize the entropy under the constraint that the first and second moments of the distribution are specified. The first moment of the distribution is parameterized by the center of gravity of the power spectrum, while the second moments are characterized by the parameters describing the concentration and the dependence of the spreads among dispersion dimensions.

In this contribution, we propose to use the Fisher-Bingham-5 (FB_5) density function to describe the shape of the elevation-azimuth power spectrum of individual path components. The maximum likelihood (ML) estimator of the parameters of the power spectrum is derived and applied to extract the dispersive characteristics of individual path components from measurement data.

The organization of this contribution is as follows. In Section II, the FB_5 density function is introduced. In Section III, the signal model for the channel sounding is presented. Section IV shows the preliminary results of

This work was jointly supported by the Network of Excellence in Wireless COMmunications (NEWCOM) and Elektrobit Group.

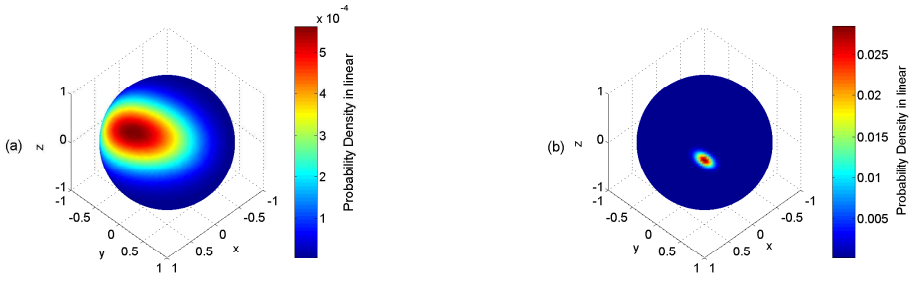

	$\bar{\phi}$ [°]	$\bar{\theta}$ [°]	α [°]	κ	β
(a)	0	45	160	5	1.5
(b)	45	70	35	200	100

Fig. 1. The FB_5 density functions calculated using (2) with parameter settings given above.

experimental investigations. Finally concluding remarks are stated in Section V.

II. Fisher-Bingham-5 Density Function

Following the nomenclature in [7], a direction can be characterized using a unit vector $\mathbf{\Omega}$. This vector has its initial point anchored at the origin O of a coordinate system specified in the region surrounding the array of interest, and terminal point located on a unit sphere $\mathbb{S}_2$ centered at O. This vector is uniquely determined by its elevation $\theta \in [0, \pi]$ and azimuth $\phi \in [-\pi, +\pi)$ according to

$$\mathbf{\Omega} = \boldsymbol{e}(\theta, \phi) \doteq \begin{bmatrix} \cos(\phi)\sin(\theta) \\ \sin(\phi)\sin(\theta) \\ \sin(\theta) \end{bmatrix}. \tag{1}$$

Among all distributions on the unit sphere $\mathbb{S}_2$, the FB_5 distribution [8] maximizes the entropy under the constraints that the first moment of the distribution and its second moment are specified. The density function of the FB_5 distribution is of the form [8]

$$f_{\mathrm{FB}_5}(\mathbf{\Omega}) = C(\kappa,\beta)^{-1}\exp\{\kappa\boldsymbol{\gamma}_1^{\mathrm{T}}\mathbf{\Omega} + \beta[(\boldsymbol{\gamma}_2^{\mathrm{T}}\mathbf{\Omega})^2 - (\boldsymbol{\gamma}_3^{\mathrm{T}}\mathbf{\Omega})^2]\}, \tag{2}$$

where $\kappa \geq 0$ and $\beta \in [0, \kappa/2)$ are respectively the concentration parameter and the ovalness parameter of the distribution, and $C(\kappa, \beta)$ denotes a normalization constant number depending on κ and β. In (2), $\boldsymbol{\gamma}_1$, $\boldsymbol{\gamma}_2$ and $\boldsymbol{\gamma}_3 \in \mathbb{R}^{3\times 1}$ are unit vectors. The matrix

$$\mathbf{\Gamma} \doteq [\boldsymbol{\gamma}_1, \boldsymbol{\gamma}_2, \boldsymbol{\gamma}_3]$$

is uniquely determined by three angular parameters $\bar{\theta}$, $\bar{\phi}$ and α according to

$$\begin{aligned} \mathbf{\Gamma} &= \begin{bmatrix} \sin(\bar{\theta})\cos(\bar{\phi}) & -\sin(\bar{\phi}) & \cos(\bar{\theta})\cos(\bar{\phi}) \\ \sin(\bar{\theta})\sin(\bar{\phi}) & \cos(\bar{\phi}) & \cos(\bar{\theta})\sin(\bar{\phi}) \\ \cos(\bar{\theta}) & 0 & -\sin(\bar{\theta}) \end{bmatrix} \\ &\quad \cdot \begin{bmatrix} 1 & 0 & 0 \\ 0 & \cos(\alpha) & -\sin(\alpha) \\ 0 & \sin(\alpha) & \cos(\alpha) \end{bmatrix}. \end{aligned} \tag{3}$$

In (3), $\bar{\theta}$ and $\bar{\phi}$ coincide with respectively the elevation and the azimuth of the mean direction, i.e. the first moment of the distribution. The angle α describes how the density function is tilted on the unit sphere $\mathbb{S}_2$. A more illustrative description of the meanings of $\boldsymbol{\gamma}_1$, $\boldsymbol{\gamma}_2$ and $\boldsymbol{\gamma}_3$ can be found in [8].

Fig. 1 depicts the graphs calculated using the FB_5 density function on $\mathbb{S}_2$ for two parameter settings which are also reported in this figure. The elevation-azimuth density function $f_{\mathrm{FB}_5}(\theta, \phi)$ can be derived from $f_{\mathrm{FB}_5}(\mathbf{\Omega})$ in (2) via the mapping $[\theta, \phi] \mapsto \boldsymbol{e}(\theta, \phi)$:

$$\begin{aligned} f_{\mathrm{FB}_5}(\theta,\phi) &= f_{\mathrm{FB}_5}(\mathbf{\Omega}) \cdot \det(\boldsymbol{J}(\theta,\phi)) \\ &= C(\kappa,\beta)^{-1}\sin(\theta)\cdot\exp\{\kappa\boldsymbol{\gamma}_1^{\mathrm{T}}\boldsymbol{e}(\phi,\theta) \\ &\quad +\beta[(\boldsymbol{\gamma}_2^{\mathrm{T}}\boldsymbol{e}(\phi,\theta))^2 - (\boldsymbol{\gamma}_3^{\mathrm{T}}\boldsymbol{e}(\phi,\theta))^2]\}. \end{aligned} \tag{4}$$

Here, $\det(\cdot)$ denotes the determinant of the matrix given as an argument and $\boldsymbol{J}(\theta,\phi) = \frac{\partial \boldsymbol{e}(\phi,\theta)}{\partial(\theta,\phi)}$ is the Jacobian matrix.

III. Signal Model

In this contribution, we consider dispersion of individual path components in EoA and AoA. However, the results can be easily generalized to the case where dispersion in the elevation and azimuth of departure is considered. The condition of narrow-band transmission is assumed, which implies that the product of the signal bandwidth times the channel delay spread is much smaller than one. Following the nomenclature in [7], the continuous-time output signal of the $M-$element Rx array in an SIMO (single-input multiple-ouput) system reads

$$\begin{aligned} \boldsymbol{Y}(t) &= \boldsymbol{H}(t)u(t) + \boldsymbol{W}(t) \\ &= \left[\int_0^{\pi}\int_{-\pi}^{+\pi} \boldsymbol{c}(\phi,\theta)h(t;\theta,\phi)\mathrm{d}\phi\mathrm{d}\theta\right]u(t) + \boldsymbol{W}(t) \end{aligned} \tag{5}$$

The vector $\boldsymbol{Y}(t) \in \mathbb{C}^M$ contains the output signals of the Rx array observed at time instance t. The vector $\boldsymbol{H}(t) \in$

$\mathbb{C}^M$ represents the time-variant impulse response of the SIMO system. The $u(t)$ denotes the complex envelope of the transmitted sounding signal, which is assumed to be known to the Rx. The function $h(t;\theta,\phi)$ is referred to as the (time-variant) elevation-azimuth spread function of the propagation channel [7].

In a scenario where the electromagnetic energy propagates from the Tx to the Rx via D paths, $h(t;\theta,\phi)$ can be decomposed as

$$h(t;\theta,\phi) = \sum_{d=1}^{D} h_d(t;\theta,\phi). \tag{6}$$

The summand $h_d(t;\theta,\phi)$ denotes the dth path component in $h(t;\theta,\phi)$. The noise component $\boldsymbol{W}(t) \in \mathbb{C}^M$ in (5) is a vector-valued circularly symmetric, spatially and temporally white Gaussian process with component spectral height σ_w^2. Finally, the M-dimensional complex vector

$$\boldsymbol{c}(\phi,\theta) \doteq [c_1(\phi,\theta),\ldots,c_m(\phi,\theta),\ldots,c_M(\phi,\theta)]^{\mathrm{T}}$$

with $[\cdot]^{\mathrm{T}}$ denoting transposition is the responses of the Rx array.

We assume that the vector $\boldsymbol{H}(t)$ fluctuates over the overall sounding period, but it is constant within individual observation intervals:

$$\boldsymbol{H}(t) = \boldsymbol{H}(t_n) \doteq \boldsymbol{H}_n, \quad t \in [t_n, t_n + T).$$

Here T denotes the duration of one observation interval. Similarly, the elevation-azimuth spread function $h_d(t;\theta,\phi)$ arising in (6) is constant within individual observation intervals:

$$h_d(t;\theta,\phi) = h_d(t_n;\theta,\phi) \doteq h_{d,n}(\theta,\phi), \quad t \in [t_n, t_n + T).$$

The processes $h_{d,n}(\theta,\phi)$, $n \in [1,\ldots,N]$, $d \in [1,\ldots,D]$ with N denoting the number of the observation intervals, are uncorrelated complex (zero-mean) orthogonal stochastic measures, i.e.

$$\mathrm{E}[h^*_{d,n}(\theta,\phi)h_{d',n'}(\theta',\phi')] = P_d(\theta,\phi)\delta_{nn'}\delta_{dd'}\delta(\phi-\phi')\delta(\theta-\theta'), \tag{7}$$

where $(\cdot)^*$ denotes the complex conjugate, $\delta_{(\cdot)}$ and $\delta(\cdot)$ represent the Kronecker delta and the Dirac delta function respectively, and

$$P_d(\theta,\phi) \doteq \mathrm{E}[|h_{d,n}(\theta,\phi)|^2]$$

represents the elevation-azimuth power spectrum of the dth path component. Thus, identity (7) implies that the spread functions of different individual path components or at different observation intervals are uncorrelated. This scenario is referred to as the *incoherent-distributed-source* case in the literature (see e.g. [9]).

The spectrum $P_d(\theta,\phi)$ describes the manner in which the average power of the dth path component is distributed with respect to both AoD and AoA. We assume

$$P_d(\theta,\phi) = P_d \cdot f_d(\theta,\phi)$$

with P_d representing the total average power of the dth path component and $f_d(\theta,\phi)$ being of the form of $f_{\mathrm{FB}_5}(\theta,\phi)$ in (4) with path-specific parameters

$$\boldsymbol{\theta}_d \doteq [\bar{\phi}_d, \bar{\theta}_d, \kappa_d, \beta_d, \alpha_d].$$

We use a vector $\boldsymbol{\theta}$ to contain the model parameters in (5), i.e.

$$\boldsymbol{\theta} \doteq [\sigma_w^2, P_1, P_2, \ldots, P_D, \boldsymbol{\theta}_1, \boldsymbol{\theta}_2, \ldots, \boldsymbol{\theta}_D].$$

IV. Experimental Investigations

To assess the applicability of the proposed characterization method, we derive a stochastic maximum likelihood estimator [10] of $\boldsymbol{\theta}$ for the single-path-component scenario and apply it to the measurement data. These data were collected using the MIMO wideband radio channel sounder Propsound CS [12] [13] in a big hall environment. During the measurement procedure, the hall was crowded with people moving around. These movements introduced time variations of the channel response. A detail description of the equipment setting and the environment where the measurement was conducted can be found in [5]. The Tx and Rx were both equipped with two identical 50-element dual-polarized omni-directional antenna arrays. The positions of the Rx and Tx were kept fixed during the measurement procedure. The data from 200 measurement cycles were collected within a period of 13 seconds. A measurement cycle is referred to as the interval within which all 50×50 subchannels are sounded once.

For the preliminary study where dispersion in AoA and EoA is considered, we selected a SIMO system with one Tx antenna and a 32-element subarray of the Rx array. In the Rx subarray, 14 elements are located on the top ring of the array and 18 on its lower ring (Please refer to [5] for the illustration of the Rx array). Fig. 2 depicts a portion of the average power delay profile of the output of the Rx array by averaging the squared responses of the subchannels measured in 200 cycles.

Since dispersion in delay is not considered, we select the output of the Rx subarray at a specific delay, where the average power delay profile exhibits a peak. In this study, we consider the outputs at delay $\tau = 40$ ns and at delay $\tau = 115$ ns respectively. These outputs correspond to respectively the first and the last peaks in the power delay profile shown in Fig. 2.

Fig. 3 depicts the results obtained using the output of the Rx subarray at delay $\tau = 40$ ns. The notations in the titles of the figures are explained below:

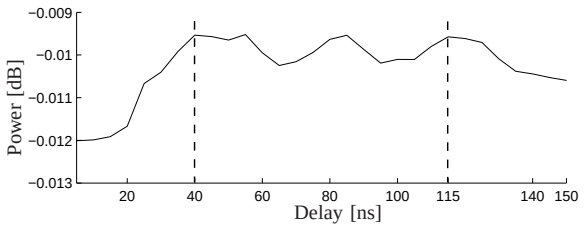

Fig. 2. Average power delay profile of the received signal.

- $\mathrm{Bartlett}(\hat{\mathbf{\Sigma}})$: the Bartlett spectrum computed with the original output of the Rx subarray,
- $\hat{P}(\phi, \theta)$: the power spectrum ML estimate of a single path component using the proposed characterization method,
- $\mathrm{Bartlett}(\mathbf{\Sigma}(\hat{\boldsymbol{\theta}}))$: the Bartlett spectrum computed with a reconstructed covariance matrix which is calculated based on the power spectrum ML estimate,
- $\hat{P}(\mathbf{\Omega})$: the ML estimate of the power spectrum illustrated on the unit sphere.

Comparing $\hat{P}(\phi, \theta)$ and $\mathrm{Bartlett}(\mathbf{\Sigma}(\hat{\boldsymbol{\theta}}))$ in Fig. 3, we observe that the power spectrum ML estimate is more concentrated than the corresponding footprint in the Bartlett spectrum. The blurring effect observed in the Bartlett spectrum is due to the ambiguity function of the Rx subarray response. As the Rx subarray consists of the antennas on the top ring and the bottom ring of the array, the ambiguity function exhibits two dominant lobes separated by about 50° in elevation. We also observe that $\mathrm{Bartlett}(\mathbf{\Sigma}(\hat{\mathbf{\Theta}}))$ is similar with $\mathrm{Bartlett}(\mathbf{\Sigma}(\boldsymbol{\theta}))$.

From $\mathrm{Bartlett}(\mathbf{\Sigma}(\hat{\mathbf{\Theta}}))$ and $\mathrm{Bartlett}(\mathbf{\Sigma}(\boldsymbol{\theta}))$ in Fig. 3 we observe that, the shapes and the maximum spectral heights of the corresponding footprints are not exactly the same. These differences may be due to the following reasons. One reason is that the FB_5 density function only provides an approximation to the shape of the effective power spectrum of individual path components. Estimation errors might result in the case where the difference is significant. Another reason that may lead to these differences is that the ML estimator only estimates the power spectrum of a single path component. It can be visually identified from $\mathrm{Bartlett}(\mathbf{\Sigma}(\boldsymbol{\theta}))$ that the scenario considered might contain two or more path components. In such a case, estimation errors may result due to the discrepancy in the number of path components in the effective received signal and this number assumed in the ML estimation.

Fig. 4 depicts the results obtained using the output of the Rx subarray at delay $\tau = 115$ ns. Similar phenomena can be observed as those obtained from Fig. 3. More specifically, $\mathrm{Bartlett}(\mathbf{\Sigma}(\hat{\mathbf{\Theta}}))$ and $\mathrm{Bartlett}(\mathbf{\Sigma}(\boldsymbol{\theta}))$ are more similar with each other than that observed from Fig. 3. This might be due to the reason that in the scenario with delay $\tau = 115$ ns, the output of the Rx subarray can be contributed by one path component scenario.

It is worth mentioning that due to the property expressed in (7), i.e. the spread functions of distinct path components are independent, the SAGE algorithm [11] can be implemented as a low-complexity approximation of the maximum likelihood estimators for the multiple-path-component scenario. The results obtained will be reported in a forth-coming paper.

V. Conclusions

In this contribution, we proposed to use the Fisher-Bingham-5 density function to model the shape of the elevation-azimuth power spectrum of individual path components. We derived the maximum likelihood estimator of the parameters of the power spectrum and used it to estimate the dispersive characteristics of individual path components from measurement data. From some preliminary results, we found that the estimated power spectra of the path components are noticeably more concentrated than the corresponding footprints in the Bartlett spectrum. The Bartlett spectrum of the covariance matrix computed based on the estimated power spectrum is similar with the Bartlett spectrum of the original data. These results demonstrated that the proposed characterization method is applicable in real situations.

VI. Acknowledgement

The authors would like to acknowledge Nels Løgsted Rohde, Svend Aage Vedstesen and Xi Fu for their project work related to the study addressed in this paper. The authors also would like to thank Troels Pedersen for discussions and comments.

References

[1] O. Besson and P. Stoica, "Decoupled estimation of DoA and angular spread for spatially distributed sources," *IEEE Trans. Signal Processing*, vol. 49, pp. 1872–1882, 1999.

[2] T. Trump and B. Ottersten, "Estimation of nominal direction of arrival and angular spread using an array of sensors," *Signal Processing*, vol. 50, pp. 57–69, Apr. 1996.

[3] C. B. Ribeiro, E. Ollila, and V. Koivunen, "Stochastic maximum likelihood method for propagation parameter estimation," in *Proceedings of the 15th IEEE International Symposium on Personal, Indoor and Mobile Radio Communications (PIMRC)*, vol. 3, Sept. 5-8 2004.

[4] C. B. Ribeiro, A. Richter, and V. Koivunen, "Stochastic maximum likelihood estimation of angle- and delay-domain propagation parameters," in *Proceedings of the 16th IEEE International Symposium on Personal, Indoor and Mobile Radio Communications (PIMRC)*, Berlin, Germany, 2005.

[5] X. Yin, T. Pedersen, N. Czink, and B. H. Fleury, "Parametric characterization and estimation of bi-azimuth dispersion of path components," in *Proceedings of the 7th IEEE International Workshop on Signal Processing Advances for Wireless Communications (SPAWC)*, Nice, France, July 2006.

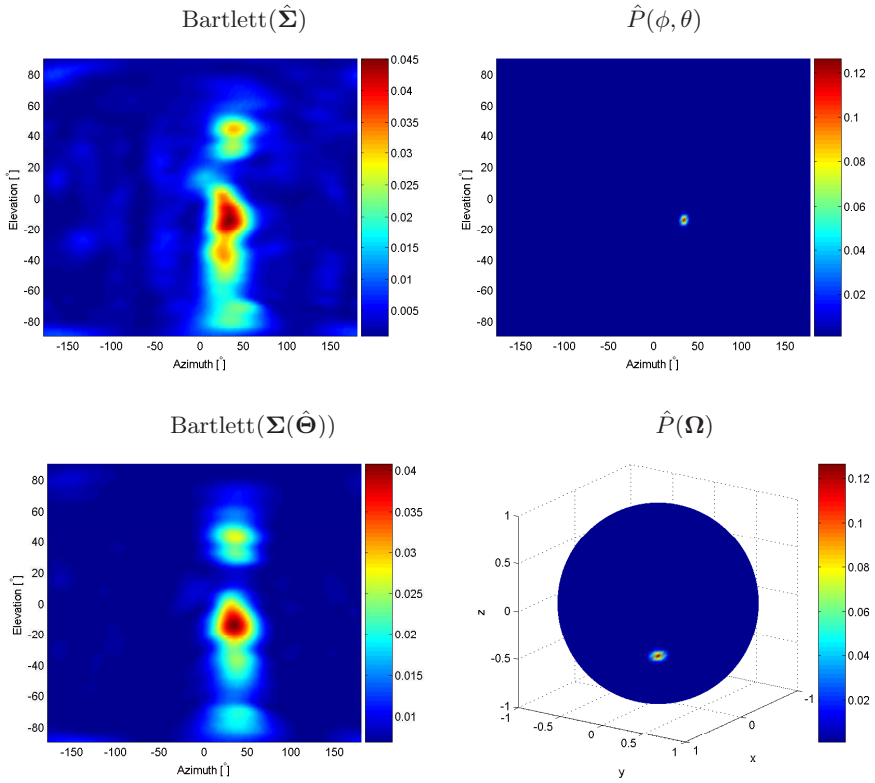

Fig. 3. Estimated elevation-azimuth power spectra at delay $\tau = 40$ ns. Color bars to the right of these plots show spectral heights expressed in linear scale.

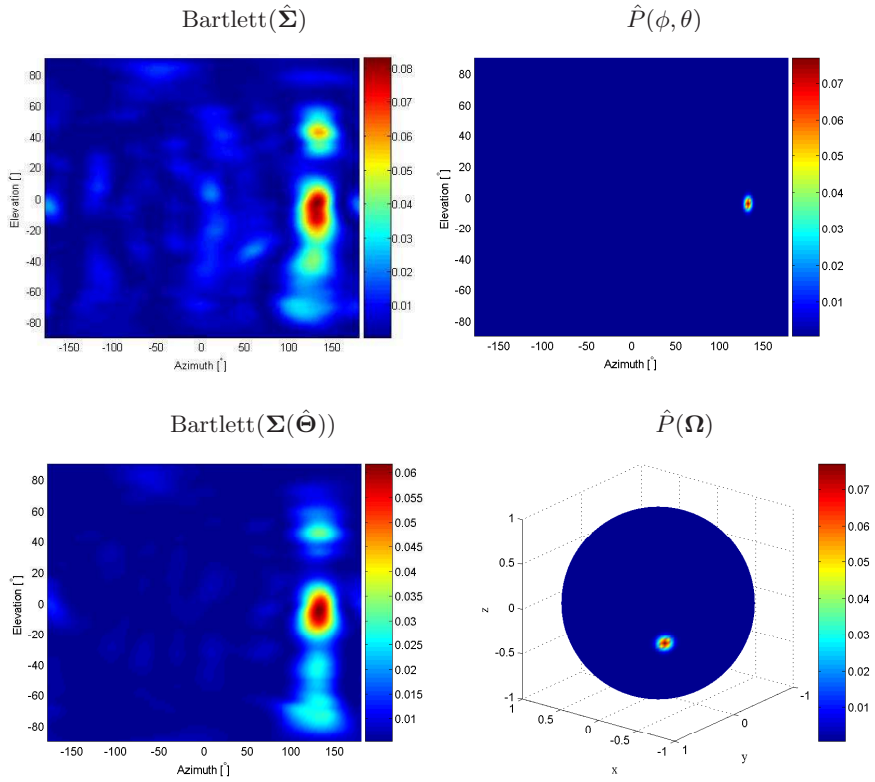

Fig. 4. Estimated elevation-azimuth power spectra at delay $\tau = 115$ ns. Color bars to the right of these plots show spectral heights expressed in linear scale.

[6] ——, “Parametric characterization and estimation of bi-azimuth and delay dispersion of path components,” in *Proceedings of The First European Conference on Antennas and Progation (EuCAP)*, Acropolis, Nice, France, November 2006.
[7] B. H. Fleury, “First- and second-order characterization of direction dispersion and space selectivity in the radio channel,” *IEEE Trans. Information Theory*, no. 6, pp. 2027–2044, Sept. 2000.
[8] J. T. Kent, “The fisher-bingham distribution on the sphere,” *Journal of the Royal Statistical Society, Serieal B (Methodological)*, vol. 44, pp. 71–80, 1982.
[9] S. Shahbazpanahi, S. Valaee, and M. Bastani, “Distributed source localization using ESPRIT algorithm,” *IEEE Transactions on Signal Processing*, vol. 49, no. 10, pp. 2169–2178, 2001.
[10] H. Krim and M. Viberg, “Two decades of array signal processing research: the parametric approach,” *IEEE Trans. Signal Processing*, vol. 13, pp. 67–94, 1996.
[11] B. H. Fleury, M. Tschudin, R. Heddergott, D. Dahlhaus, and K. L. Pedersen, “Channel parameter estimation in mobile radio environments using the SAGE algorithm,” *IEEE Journal on Selected Areas in Communications*, vol. 17, no. 3, pp. 434–450, Mar. 1999.
[12] N. Czink, E. Bonek, X. Yin, and B. H. Fleury, “Cluster angular spreads in a MIMO indoor propagation environment,” in *Proceedings of the 16th IEEE International Symposium on Personal, Indoor and Mobile Radio Communications (PIMRC)*, Berlin, Germany, 2005.
[13] E. Bonek, N. Czink, V. M. Holappa, M. Alatossava, L. Hentilä, J. Nuutinen, and A. Pal, “Indoor MIMO measurements at 2.55 and 5.25 GHz - a comparison of temporal and angular characteristics,” in *Proceedings of the 15th IST Mobile Summit*, 2006.